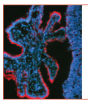
EXTENDED PDF FORMAT
SPONSORED BY

Travel Grants Available
9th FENS Forum of Neuroscience
Application Deadline:
April 30 Apply Now
RD
www.rndsystems.com



Ubiquitous Interplay Between Charge Ordering and High-Temperature Superconductivity in Cuprates

Eduardo H. da Silva Neto *et al.*

Science **343**, 393 (2014);
DOI: 10.1126/science.1243479

This copy is for your personal, non-commercial use only.

If you wish to distribute this article to others, you can order high-quality copies for your colleagues, clients, or customers by clicking here.

Permission to republish or repurpose articles or portions of articles can be obtained by following the guidelines here.

The following resources related to this article are available online at www.sciencemag.org (this information is current as of March 30, 2014):

Updated information and services, including high-resolution figures, can be found in the online version of this article at:
http://www.sciencemag.org/content/343/6169/393.full.html

Supporting Online Material can be found at:
http://www.sciencemag.org/content/suppl/2013/12/19/science.1243479.DC1.html

This article **cites 30 articles**, 5 of which can be accessed free:
http://www.sciencemag.org/content/343/6169/393.full.html#ref-list-1

This article appears in the following **subject collections:**
Physics
http://www.sciencemag.org/cgi/collection/physics

Downloaded from www.sciencemag.org on March 30, 2014

Science (print ISSN 0036-8075; online ISSN 1095-9203) is published weekly, except the last week in December, by the American Association for the Advancement of Science, 1200 New York Avenue NW, Washington, DC 20005. Copyright 2014 by the American Association for the Advancement of Science; all rights reserved. The title *Science* is a registered trademark of AAAS.

Ubiquitous Interplay Between Charge Ordering and High-Temperature Superconductivity in Cuprates

Eduardo H. da Silva Neto,[1]*† Pegor Aynajian,[1]*‡ Alex Frano,[2,3] Riccardo Comin,[4] Enrico Schierle,[3] Eugen Weschke,[3] András Gyenis,[1] Jinsheng Wen,[5] John Schneeloch,[5,6] Zhijun Xu,[5] Shimpei Ono,[7] Genda Gu,[5] Mathieu Le Tacon,[2] Ali Yazdani[1]§

Besides superconductivity, copper-oxide high-temperature superconductors are susceptible to other types of ordering. We used scanning tunneling microscopy and resonant elastic x-ray scattering measurements to establish the formation of charge ordering in the high-temperature superconductor $Bi_2Sr_2CaCu_2O_{8+x}$. Depending on the hole concentration, the charge ordering in this system occurs with the same period as those found in Y-based or La-based cuprates and displays the analogous competition with superconductivity. These results indicate the similarity of charge organization competing with superconductivity across different families of cuprates. We observed this charge ordering to leave a distinct electron-hole asymmetric signature (and a broad resonance centered at +20 milli–electron volts) in spectroscopic measurements, indicating that it is likely related to the organization of holes in a doped Mott insulator.

Understanding the mechanism of superconductivity and its interplay with other possible spin or charge organizations in high–transition temperature (T_c) cuprate superconductors remains one of the greatest challenges in condensed matter physics. The observation in La-based cuprates of a suppression of T_c near $x = 1/8$ doping (hole/Cu) coinciding with the organization of charge into stripe-like patterns with four lattice constants (4a) periodicity provided early evidence that charge ordering (CO) competes with superconductivity (*1*, *2*). Recently, x-ray scattering experiments on highly ordered Y-based cuprates have discovered that in the same range of hole concentration (near $x = 1/8$), there is a competing charge organization with an incommensurate ordering vector (≈ 3.3a periodicity) (*3*, *4*). These experiments raise the question of whether there is a universal CO mechanism common to all underdoped cuprates [although crystalline structures in each compound may modify details of the resulting ordering patterns (*5*, *6*)]. If there is a connection between the observed COs in different compounds, what is the mechanism by which this phenomenon competes or is intertwined with high-T_c superconductivity (*7*)? Do strong correlations, such as those present as a result of proximity to the Mott insulator, play a role in the CO state and its interplay with superconductivity?

To address these questions, we have carried out scanning tunneling microscopy (STM) and spectroscopy, as well as resonant elastic x-ray scattering (REXS) measurements, on underdoped $Bi_2Sr_2CaCu_2O_{8+x}$ (Bi-2212) samples. The Bi-2212 system is the only material system among the cuprates for which there is detailed spectroscopic information on the Fermi surface and the occupied electronic states as a function of temperature and doping, obtained from angle-resolved photoemission spectroscopy (ARPES) performed over the past two decades (*8*–*10*). Yet, ARPES measurements have not shown any evidence of band folding associated with CO along the Cu-O bond direction in this system (*9*, *11*, *12*). STM studies have long reported evidence of spatial modulation of electronic states in Bi-based cuprates (*13*–*19*), but evidence for CO in these experiments is often obfuscated by the disorder-induced energy-dispersive quasiparticle interference (QPI) effect (*19*–*21*). The analysis of STM conductance maps over a range of energies has been used to provide evidence for fluctuating charge organization in Bi-2212 below T^*, with strongest enhancement near 1/8 doping—the same doping range in which charge organizations have been seen in Y- and La-based cuprates (*19*). However, it remains a challenge to clearly separate signatures of CO from those of QPI in STM experiments and, more importantly, to corroborate the surface-sensitive measurements with bulk-sensitive experiments. Here, we provide high-resolution energy-revolved STM spectroscopy experiments that clearly distinguish between QPI and CO features as a function of doping and temperature; this CO signature is also detected in our temperature-dependent REXS measurements.

The geometry of the combined experimental approach for examining CO in underdoped Bi-2212 samples is shown in Fig. 1A, in which we contrast the discrete Fourier transform of STM conductance maps with bulk scattering results from REXS. A typical example of a STM conductance map is shown in Fig. 1B for a UD45 (underdoped Bi-2212, $T_c = 45$ K) sample at 30 K. The discrete Fourier transform of the conductance map (Fig. 1, C and D) shows a strong peak of wave vector $\boldsymbol{q} = (\pm\delta, 0)2\pi/a$ and $(0, \pm\delta)2\pi/b$, and $\delta \approx 0.3$, along the Cu-O bond directions, corresponding to the real space modulations in Fig. 1B. The results from REXS measurements (incident photon energy of 931.5 eV, resonant with the Cu L_3-edge) on the same sample are shown in Fig. 1, E and F, as a function of the component of momentum transfer along the a direction (Fig. 1A) (*22*). The low-temperature REXS measurement (Fig. 1E) shows a peak at the same incommensurate wave vector ($\delta \approx 0.3$) as those in the discrete Fourier transform of the STM conductance maps (Fig. 1, C and D), establishing that the STM modulations on the surface of Bi-2212 sample are in fact due to a CO that can also be detected in the bulk [a similar finding on Bi-2201 is provided in (*23*)].

To understand why such a CO phenomenon has remained undetected in ARPES studies and to reveal a key spectroscopic characteristic of this ordering, we examined the energy dependence of STM conductance maps. The energy evolution of the features in the discrete Fourier transform of the conductance maps is shown in Fig. 2, along the Cu-O bond direction, measured at 30 K for a range of doping, from optimally doped (OP91) to strongly underdoped (UD15) samples. In the optimally doped sample (Fig. 2A) at temperatures well below T_c, the energy–wave vector structure along the Cu-O bond direction shows no sign of CO. Instead, it shows an energy-dispersing particle-hole symmetric wave vector originating from disorder-induced scattering interference of superconducting Boguliobov-de Gennes quasiparticles (BdG-QPI) (*13*, *18*, *19*, *24*). Reducing the doping toward the underdoped regime (Fig. 2, A to G), we found that the BdG-QPI features are systematically weakened, whereas a separate nondispersive modulation with a relatively sharp wave vector appears and strengthens peaking near UD35 (Fig. 2F). This wave vector (for example, $\delta = 0.3$ in Fig. 2, E to G) corresponds to the CO wave vector we find in the REXS measurements (Fig. 1E and fig. S7). The widths in momentum of this CO peak [full width at half maximum, $2\Gamma \approx 0.04$ reciprocal lattice units (rlu)], which agree well with our REXS measurements ($2\Gamma \approx 0.05$ rlu, or equivalently 20a in real space), are larger than those recently observed in the Y-based cuprates (*3*) and indicate a rather short-range order. Our energy-resolved STM conductance maps further show that these CO modulations only appear over a range of energies (0 to 50 meV) above the chemical potential, a behavior not expected in a conventional

[1]Joseph Henry Laboratories and Department of Physics, Princeton University, Princeton, NJ 08544, USA. [2]Max-Planck-Institut für Festkörperforschung, Heisenbergstrasse 1, D-70569 Stuttgart, Germany. [3]Helmholtz-Zentrum Berlin für Materialien und Energie, Albert-Einstein-Strasse 15, D-12489 Berlin, Germany. [4]Department of Physics and Astronomy, University of British Columbia (UBC), Vancouver, British Columbia V6T 1Z1, Canada. [5]Condensed Matter Physics and Materials Science, Brookhaven National Laboratory (BNL), Upton, NY 11973 USA. [6]Department of Physics and Astronomy, Stony Brook University, Stony Brook, NY 11794-3800, USA. [7]Central Research Institute of Electric Power Industry, Komae, 201-8511 Tokyo, Japan.

*These authors contributed equally to this work.
†Present address: Quantum Matter Institute, Department of Physics and Astronomy, University of British Columbia, Vancouver, British Columbia V6T 1Z4, Canada.
‡Present address: Department of Physics, Applied Physics and Astronomy, Binghamton University, Binghamton, NY 13902, USA.
§Corresponding author. E-mail: yazdani@princeton.edu

charge-density-wave (CDW) order. Despite being broad in energy, we found the intensity of the CO feature to be centered at ~+20 meV above the chemical potential at all doping levels (Fig. 2H). The particle-hole asymmetry of the CO feature in the STM data clearly distinguishes it from the BdG-QPI signals and explains the absence of such CO features in the ARPES studies.

The CO wave vectors extracted from our STM measurements show distinct similarities to other families of the cuprates. For a hole concentration of $x < 0.1$, the incommensurate CO wave vector $\delta \approx 0.3$ matches the CDW observed in the Y-based cuprates, whereas for $x > 0.1$, the nearly commensurate wave vector $\delta \approx 0.25$ is very similar to that found in the stripe phase of La-based cuprates (Fig. 2H). Although an incommensurate δ and its decrease with doping are expected from a Fermi surface nesting mechanism, the narrow doping range over which the jump in δ occurs in Bi-2212 may be an indication of possible competition between two different stable forms of CO in the cuprates. More broadly, though, the fact that CO in Bi-2212, in a range of doping without any structural distortion, can be either similar to Y- or La-based cuprates demonstrates our key point that CO is a ubiquitous phenomenon to underdoped cuprates.

Further evidence that connects measurements on Bi-2212 to other cuprates and probes the interplay between CO and superconductivity comes from examining the temperature dependence of the REXS and STM data. The CO signature in our REXS measurements is first detected at relatively high temperatures (Fig. 1F). By lowering the temperature, the intensity of the CO increases only down to T_c, below which it gradually weakens, suggesting a competition with superconductivity. More detailed signatures of the interplay between CO and superconductivity are observed in our STM measurements as a function of temperature for a UD75 sample (in which temperatures much lower than T_c can be accessed in our experiments). The CO signature above the chemical potential (near $\delta \approx 0.25$ for this sample) is very strong at temperatures just above T_c (Fig. 3A), while being nearly absent when the sample is cooled to roughly $0.15*T_c$ (Fig. 3D). Instead, at low temperatures, as shown in Fig. 3D, the STM data for this weakly underdoped sample recover the particle-hole-symmetric dispersing features that are due to BdG-QPI, which is consistent with a d-wave superconducting gap (*25*). This trend is analogous to the doping-dependent STM data of Fig. 2, in which the CO (measured at a constant temperature, $T = 30$ K) peaks at the UD35 sample (where $T \approx T_c$). Together, these findings not only clearly show superconductivity wins over CO at low temperatures but also provide key information about this competition in momentum space.

Previous analyses of impurity-induced QPI data at low temperatures, such as the data displayed in Fig. 3D, associated the observed dispersing wavevectors along the Cu-O bond direction with the scattering of BdG quasiparticles between points on the Fermi surface. A schematic Fermi surface for a Bi-2212 UD75 sample is shown in Fig. 3E together with the different QPI wave vectors connecting different segments of the Fermi surface, starting from near the antinodes at large

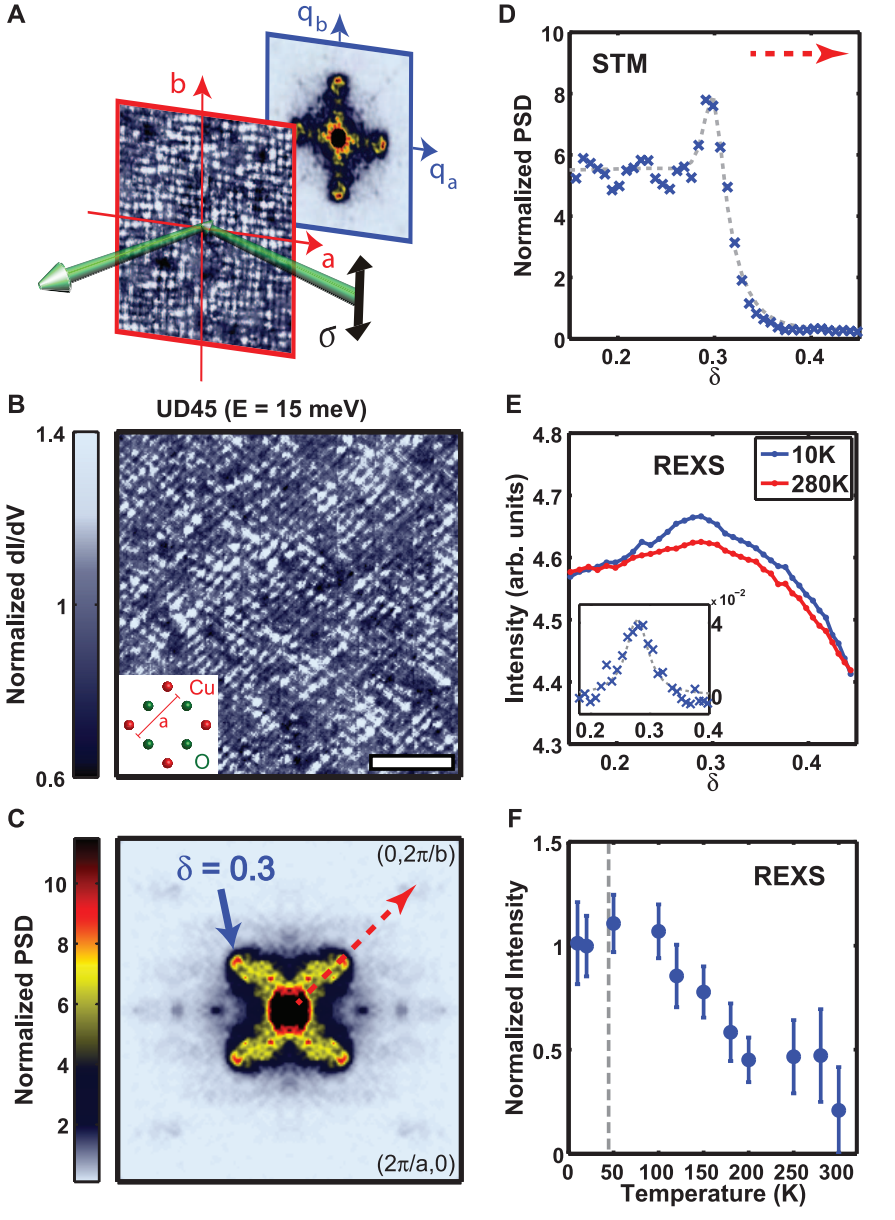


Fig. 1. CO in Bi-2212. (**A**) Schematic of the combined experimental STM-REXS approach. REXS experiments were performed with vertically polarized photons (σ) in a horizontal scattering geometry (*22*) and yield momentum space information corresponding to the real space modulations seen by STM (front) or, more directly, to the discrete Fourier transform of the STM real space data (back). We use the tetragonal crystal structure, where $a = b \approx 3.8$ Å represents the nearest neighbor Cu-Cu distance. (**B**) STM conductance map (15 meV, normalized to its spatial average) on a UD45 sample measured at 30 K. (Inset) The direction of the Cu-O-Cu bond direction relative to the measurement. Scale bar, 140 Å. (**C**) Discrete Fourier transform of the conductance map in (B); the corners of the image represent the atomic Bragg peaks at ($\pm 2\pi/a$, 0) and (0, $\pm 2\pi/b$). The discrete Fourier transform is mirror-symmetrized and normalized to its average value. The color scale represents the power spectral density (PSD) normalized to the $\delta = 0.3$ peak (blue arrow), which corresponds to the real space modulations seen in (B). The central peak ($\delta < 0.2$) corresponds to long wavelength inhomogeneity of the conductance map. (**D**) Line-cut of the energy-integrated (0 to 50 meV) discrete Fourier transform along the Cu-O bond direction [(C), red arrow] showing a clear peak at $\delta = 0.30$. Dashed line represents fit to a Lorentzian plus a background (*22*). (**E**) REXS δ-scans (*22*) for positive δ at low (blue) and high (red) temperatures on the same sample as in (B), showing a clear enhancement near $\delta = 0.3$ at low temperatures. (Inset) Background subtracted 10 K data, where the dashed line represents a Lorentzian fit to the data (*22*), in the same units as (E). (**F**) The REXS intensity extracted from the background-subtracted peak maxima as a function of temperature (*22*). The vertical dashed line corresponds to $T_c = 45$ K.

energies (small δ) to points near the nodes at low energies (large δ) (*13*, *18*, *24*, *25*). The Fermi surface of this sample, like other underdoped cuprates, is gapped at the antinodal region because of the formation of the pseudogap at high temperatures T^* (which is well above T_c for this sample). Contrasting STM data above and well below T_c shows, first, that the same quasiparticles involved in the CO at high temperature are associated with superconducting pairing at low temperatures and, second, that those quasiparticles occupy regions near the ends of the Fermi arcs (Fig. 3E) (*22*, *23*). The fact that such a competition occurs away from the antinodes suggests that charge organization is secondary to the formation of the pseudogap phase (*19*).

The unusual appearance of CO only when tunneling electrons into the sample from the STM tip (only for energies above the chemical potential), and its absence in ARPES studies, suggests that the nature of this organization is related to the strong electronic correlations, which have long been predicted to give rise to asymmetric tunneling in the doped Mott insulators (*26*, *27*). In a simplified picture, if holes doped in a Mott insulator organize into patterns, tunneling electrons into the sample at low energies would be much easier into the hole sites as opposed to electron sites because double occupancy is energetically unfavorable. In contrast, tunneling electrons out of the sample can easily occur at any site because either electrons are already present or can hop there from a nearby site on the lattice. Whether such constraints on the tunneling processes in a Mott system can explain the broad resonance (+20 meV) that we observe above the Fermi energy (which is remarkably independent of doping) requires further investigations. Overall, although much remains to be understood about the underlying mechanism of CO or its unusual characteristics reported here, its universality across cuprate families establishes it as a critical component for understanding the electronic properties and superconductivity of high-T_c cuprates.

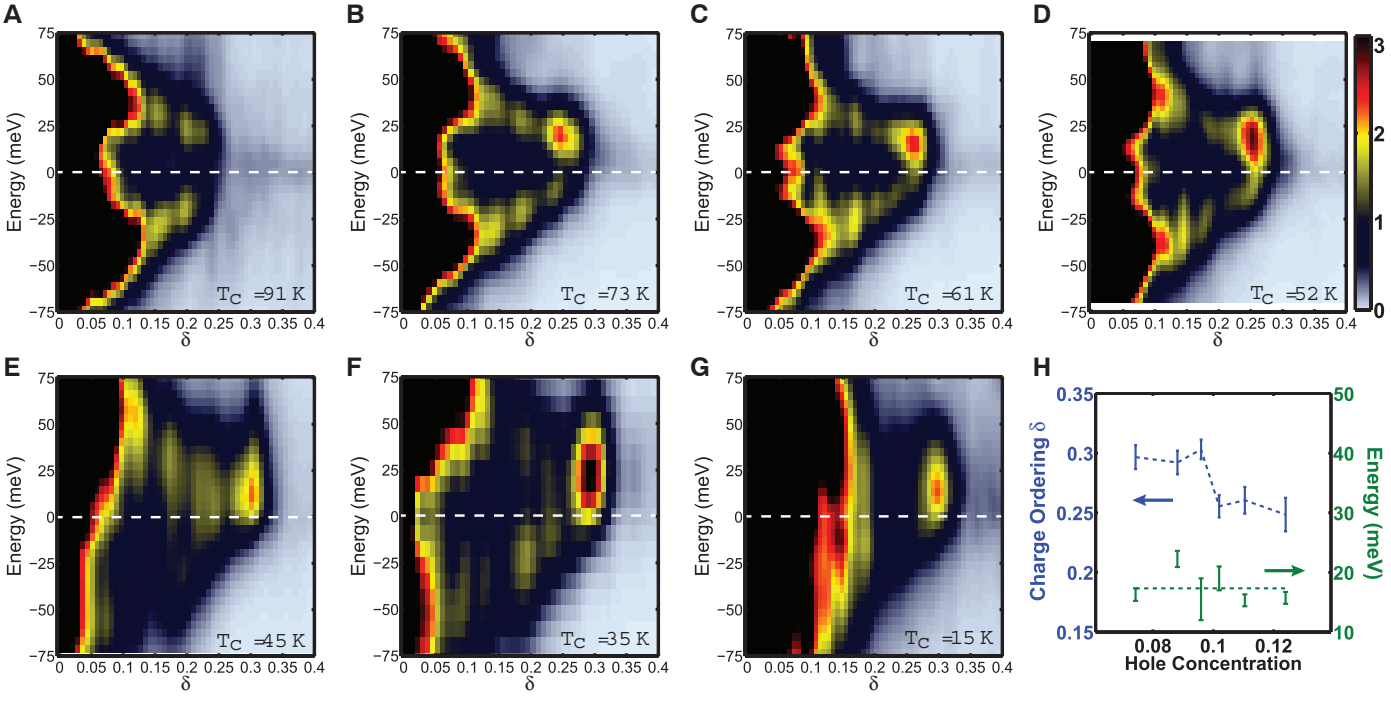


Fig. 2. Doping dependence of the STM data. (**A** to **G**) Energy-momentum structure of the modulations seen in STM along the Cu-O bond direction, extracted from line cuts along the (2π/a, 0) direction of the discrete Fourier transforms measured at 30 K for different doping levels (*22*). (**H**) Energy and δ location of the CO feature as a function of doping, extracted from energy-integrated δ cuts (*22*). The error bars in δ represent the half width at half maximum of the extracted peaks. The error bars in energy represent the SE obtained from a least-squares fit to a Lorentzian. The green dashed line represents the energy location averaged from all dopings.

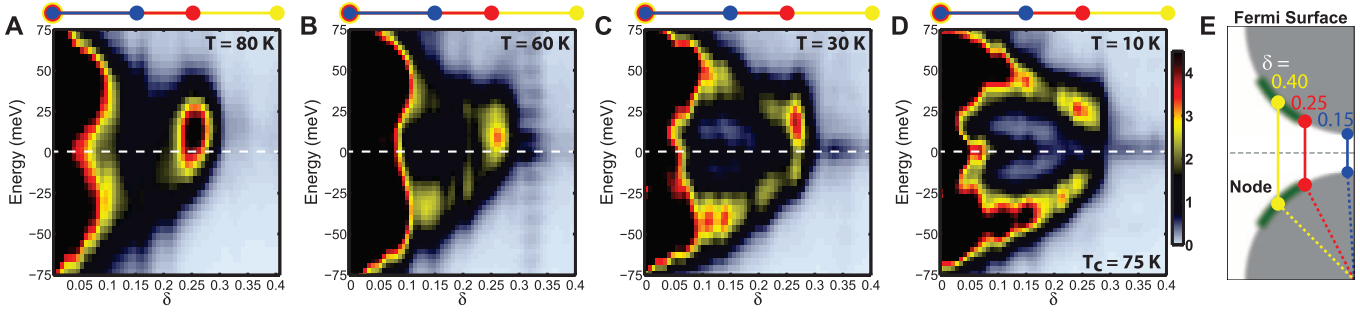


Fig. 3. Temperature dependence of the STM data. (**A** to **D**) Energy-momentum structure of the modulations seen in STM along the Cu-O bond direction, extracted from line cuts along the (2π/a, 0) direction of the discrete Fourier transforms for a UD75 sample measured at selected temperatures. The data show the opposite temperature dependence between the particle-hole symmetric BdG-QPI and the particle-hole asymmetric CO. (**E**) Schematic layout of the Fermi surface in Bi-2212 UD75 sample. The green segments represent the Fermi arc as determined by ARPES above T_c (*22*, *28*). The vertical lines [also reproduced horizontally in (A) to (D)] correspond to QPI wave vectors connecting the Fermi surface [which is consistent with ARPES (*22*, *29*)] at different regions.

References and Notes

1. J. M. Tranquada, B. J. Sternlieb, J. D. Axe, Y. Nakamura, S. Uchida, *Nature* **375**, 561–563 (1995).
2. P. Abbamonte *et al.*, *Nat. Phys.* **1**, 155–158 (2005).
3. G. Ghiringhelli *et al.*, *Science* **337**, 821–825 (2012).
4. J. Chang *et al.*, *Nat. Phys.* **8**, 871–876 (2012).
5. R. J. Cava, A. Santoro, D. W. Johnson, W. W. Rhodes, *Phys. Rev. B* **35**, 6716–6720 (1987).
6. B. Büchner, M. Breuer, A. Freimuth, A. P. Kampf, *Phys. Rev. Lett.* **73**, 1841–1844 (1994).
7. E. Fradkin, S. A. Kivelson, *Nat. Phys.* **8**, 864–866 (2012).
8. H. Ding *et al.*, *Phys. Rev. Lett.* **78**, 2628–2631 (1997).
9. A. Damascelli, Z. Hussain, Z.-X. Shen, *Rev. Mod. Phys.* **75**, 473–541 (2003).
10. H. B. Yang *et al.*, *Nature* **456**, 77–80 (2008).
11. A. Mans *et al.*, *Phys. Rev. Lett.* **96**, 107007 (2006).
12. U. Chatterjee *et al.*, *Phys. Rev. Lett.* **96**, 107006 (2006).
13. J. E. Hoffman *et al.*, *Science* **297**, 1148–1151 (2002).
14. C. Howald, H. Eisaki, N. Kaneko, A. Kapitulnik, *Proc. Natl. Acad. Sci. U.S.A.* **100**, 9705–9709 (2003).
15. M. Vershinin *et al.*, *Science* **303**, 1995–1998 (2004).
16. T. Hanaguri *et al.*, *Nat. Phys.* **3**, 865–871 (2007).
17. W. D. Wise *et al.*, *Nat. Phys.* **4**, 696–699 (2008).
18. Y. Kohsaka *et al.*, *Nature* **454**, 1072–1078 (2008).
19. C. V. Parker *et al.*, *Nature* **468**, 677–680 (2010).
20. S. A. Kivelson *et al.*, *Rev. Mod. Phys.* **75**, 1201–1241 (2003).
21. E. H. da Silva Neto *et al.*, *Phys. Rev. B* **85**, 104521 (2012).
22. Materials and methods are available as supplementary materials on *Science* Online.
23. R. Comin *et al.*, *Science* **343**, 390–392 (2013).
24. T. Hanaguri *et al.*, *Science* **323**, 923–926 (2009).
25. Q.-H. Wang, D.-H. Lee, *Phys. Rev. B* **67**, 020511 (2003).
26. P. W. Anderson, N. P. Ong, *J. Phys. Chem. Solids* **67**, 1–5 (2006).
27. M. Randeria, R. Sensarma, N. Trivedi, F.-C. Zhang, *Phys. Rev. Lett.* **95**, 137001 (2005).
28. W. S. Lee *et al.*, *Nature* **450**, 81–84 (2007).
29. I. M. Vishik *et al.*, *Nat. Phys.* **5**, 718–721 (2009).

Acknowledgments: The work at Princeton was primarily supported by a grant from the U.S. Department of Energy (DOE) Basic Energy Sciences. The instrumentation and infrastructure at the Princeton Nanoscale Microscopy Laboratory used for this work were also supported by grants from NSF-DMR1104612, the NSF–Materials Research and Engineering Center program through Princeton Center for Complex Materials (DMR-0819860), the Eric & Wendy Schmidt Transformative Fund, and the W. M. Keck Foundation. Work at BNL was supported by DOE under contract DE-AC02-98CH10886. The Max Planck–UBC Centre for Quantum Materials and Canadian Insititute for Advanced Research Quantum Materials also supported this work. We thank P. W. Anderson, E. Abrahams, S. Kivelson, S. Misra, and N. P. Ong for fruitful discussions. We also acknowledge A. Damascelli and B. Keimer for discussions and for sharing the results of their x-ray studies on Bi-2201 before publication. A.Y. acknowledges the hospitality of the Aspen Center for Physics, supported under NSF grant PHYS-1066293. The synthesis of the oxygen-doped Bi2212 samples was supported by the Center for Emergent Superconductivity, an Energy Frontier Research Center.

Supplementary Materials

www.sciencemag.org/content/343/6169/393/suppl/DC1
Materials and Methods
Figs. S1 to S9
References (*30*, *31*)

19 July 2013; accepted 25 November 2013
Published online 19 December 2013;
10.1126/science.1243479

Imaging Dynamics on the $F + H_2O \rightarrow HF + OH$ Potential Energy Surfaces from Wells to Barriers

Rico Otto,[1]* Jianyi Ma,[2,3]* Amelia W. Ray,[1] Jennifer S. Daluz,[1] Jun Li,[3] Hua Guo,[3]† Robert E. Continetti[1]†

The study of gas-phase reaction dynamics has advanced to a point where four-atom reactions are the proving ground for detailed comparisons between experiment and theory. Here, a combined experimental and theoretical study of the dissociation dynamics of the tetra-atomic FH_2O system is presented, providing snapshots of the $F + H_2O \rightarrow HF + OH$ reaction. Photoelectron-photofragment coincidence measurements of the dissociative photodetachment (DPD) of the $F^-(H_2O)$ anion revealed various dissociation pathways along different electronic states. A distinct photoelectron spectrum of stable FH–OH complexes was also measured and attributed to long-lived Feshbach resonances. Comparison to full-dimensional quantum calculations confirms the sensitivity of the DPD measurements to the subtle dynamics on the low-lying FH_2O potential energy surfaces over a wide range of nuclear configurations and energies.

Thanks to the fruitful interplay between experiment and theory, our understanding of elementary atom-diatom reactions such as $F + H_2 \rightarrow HF + H$ at the quantum mechanical level is now highly sophisticated (*1*, *2*). As the number of atoms N in a chemical reaction increases, the complexity grows dramatically as $3N-6$ coordinates are necessary to fully describe the system. With six degrees of freedom, four-atom reactions have emerged naturally as the new proving ground for understanding reaction dynamics. Recently, theoretical methods have progressed to a level where highly accurate comparisons with experimental results are becoming possible for four-atom reactions (*3*), such as the benchmark $H_2 + OH \rightarrow H_2O + H$ and its isotopologs (*4*–*7*).

One of the key foundations for analyzing a chemical reaction is a detailed knowledge of the Born-Oppenheimer potential energy surface (PES), which represents the relation between a geometrical arrangement of the nuclei of a chemical system and its corresponding electronic energy. A number of experimental techniques have been developed that are sensitive to different aspects of the molecular PES. For example, rate coefficients depend on the height of reaction barriers and/or are sensitive to the long-range forces between reactants. Molecular spectroscopy provides structural information and allows probing of different product internal states. Crossed-molecular beam measurements of angle-resolved differential cross sections map the reaction dynamics on a quantum state-to-state level (*8*) and are sensitive to dynamical (e.g., Feshbach) resonances in chemical reactions (*9*). In addition, nonadiabatic dynamics that involve transitions between multiple electronic PESs have also attracted increasing attention (*10*, *11*). Negative ion photoelectron spectroscopy has been demonstrated as an effective tool (*12*) with application to both nonadiabatic effects (*13*) and resonance phenomena (*14*). The combined information from these different sources offers a stringent test for state-of-the-art theoretical methods, advancing our understanding of chemical reactions in more complex systems. Substantial progress in the field of reaction dynamics has thereby always been closely tied to the detailed study of benchmark systems like $F + H_2$. A natural extension to consider as we move to four-atom systems is the $F + H_2O$ reaction.

The $F + H_2O$ reaction is a prototypical hydrogen abstraction reaction between a radical and water. It represents a fundamental reaction of anthropogenic fluorine in Earth's atmosphere (*15*) and may also play a key role in the formation of HF that has recently been discovered in the interstellar media (*16*). The interaction of the F atom with water gives rise to three different PESs, two of which correlate with the $F(^2P_{3/2})$ ground state (Fig. 1). In the adiabatic limit, the lower-lying ground (X) state corresponds to $HF + OH(^2\Pi_{3/2})$, whereas the higher-lying excited (A) state leads to spin-orbit excited $HF + OH(^2\Pi_{1/2})$ products (*17*). A reaction barrier separates van der Waals (vdW) complexes on the entrance and exit channel sides of the reaction (*18*, *19*). Recent theoretical studies have shown that the prereaction

[1]Department of Chemistry and Biochemistry, University of California, San Diego, 9500 Gilman Drive, La Jolla, CA 92093, USA. [2]Institute of Atomic and Molecular Physics, Sichuan University, Chengdu, Sichuan 610065, China. [3]Department of Chemistry and Chemical Biology, University of New Mexico, Albuquerque, NM 87131, USA.

*These authors contributed equally to this work.
†Corresponding author. E-mail: hguo@unm.edu (H.G.); rcontinetti@ucsd.edu (R.E.C.)